Review

Convergence of spectroscopic and kinetic electron transfer parameters for mixed-valence binuclear dipyridylamide ruthenium ammine complexes

Alison J. Distefano[a], James F. Wishart[b],*, Stephan S. Isied[a],*

[a] *Department of Chemistry and Chemical Biology, Rutgers, The State University of New Jersey, Piscataway, New Jersey 08854, USA*
[b] *Chemistry Department, Brookhaven National Laboratory, Upton, New York 11973, USA*

Contents

Abstract

A series of binuclear ruthenium(II,III) pentaammine complexes bridged by 4-pyridyl isonicotinamide (*iso*-apy) and methyl,4-pyridyl isonicotinamide (*iso*-mapy), and their mononuclear congeners, were studied by spectroscopic and kinetic techniques. The amide function-ality provides asymmetry between the electronic environments of the metal ions bound to the aminopyridine (apy) and pyridine carbonyl (*iso*) ends. The resulting difference is observed in the charge transfer spectra and the electrochemical properties of the mononuclear and binuclear complexes. The mixed-valence binuclear ruthenium(II,III) complexes exhibit bands in the NIR region assigned to intervalence charge transfer transitions between the metal centers (MMCT). The MMCT band for [(NH$_3$)$_5$Ru-*iso*-apy-Ru(NH$_3$)$_5$]$^{5+}$ has $\lambda_{\max}$ = 809 nm and

---

* Corresponding authors. Tel.: +1 631 344 4327/+1 732 445 3764; fax: +1 631 344 5815/+1 732 445 5312.
   E-mail addresses: wishart@bnl.gov (J.F. Wishart), isied@rutchem.rutgers.edu (S.S. Isied).

$\varepsilon_{max} = 50\,M^{-1}\,cm^{-1}$ and $[(NH_3)_5Ru\text{-}iso\text{-}mapy\text{-}Ru(NH_3)_5]^{5+}$ has $\lambda_{max} = 743\,nm$ and $\varepsilon_{max} = 20\,M^{-1}\,cm^{-1}$. Methylation of the amide nitrogen increases the energy of the MMCT transition while decreasing the electronic coupling between the two metal centers. The electronic coupling constants ($H_{MM'}$) for the mixed-valence complexes were evaluated from the metal-to-ligand and metal-to-metal charge transfer spectra using both Hush's model and the CNS method. The spectroscopy shows that electronic coupling is more efficient when the bridging ligand can adopt a more planar configuration. The kinetics of the spontaneous (thermal) intramolecular ET reactions in the binuclear ruthenium pentaammine systems of *iso*-mapy and *iso*-apy were studied using pulse radiolysis transient absorption spectroscopy. An ET rate constant of $2.7 \times 10^6\,s^{-1}$ was obtained for $[(NH_3)_5Ru\text{-}iso\text{-}mapy\text{-}Ru(NH_3)_5]^{5+}$, while only a lower limit for the thermal reaction rate constant could be obtained for $[(NH_3)_5Ru\text{-}iso\text{-}apy\text{-}Ru(NH_3)_5]^{5+}$. The estimated ET rate constants calculated by Hush's model are slightly faster than those directly obtained through kinetic measurements.

1. Introduction

Understanding electron transfer across extended organic bridging ligands and mixed valence chemistry is one of the main themes of Professor Taube's research [1–9]. Using a variety of 4,4′-bipyridine and similar bridging ligands, the interaction between transition metal ions of mixed oxidation states has been systematically studied using ruthenium and osmium ammine complexes as donors and acceptors. This led to the development of a rich field of charge transfer spectra assigned to metal-to-ligand (ML), ligand-to-metal (LM) and metal-to-metal (MM) transitions. From such spectral assignments, electron transfer (ET) parameters such as electronic coupling, reorganization energy and thermal rates of electron transfer can be calculated. Throughout the development of this field it was realized that examples where both a thermal ET reaction and an intervalence transfer band can be observed together are highly advantageous because they allow kinetically and spectroscopically determined electron transfer parameters to be directly compared. In this paper, we report on two such complexes where comparisons of this kind are possible.

Binuclear complexes containing bridges having terminal pyridyl groups, with similar or different spectator (non-bridging) ligands bound to the metal center, have been extensively studied [8,10–16]. By using non-bridging ligands with different π back-bonding properties, the driving force of the ET reaction in these complexes can be altered [17–20]. We report here on dipyridyl-type bridging ligands separated by amide linkages where the asymmetry in the properties of their metal complexes results from the differences between the electron donating (apy) and the electron withdrawing (iso) pyridine rings forming the amide bond. The difference between the electronic properties of these two pyridyl groups provides an opportunity to investigate ET reactions across amides with different conformations, such as those present in peptides and proteins. The small asymmetry in the electronic properties of these complexes allows one to determine both the electron transfer parameters of the light induced uphill ET reaction of the mixed-valence complex and, in a separate kinetic experiment, the thermal rate for the corresponding downhill ET reaction. By placing substituents on the amide group, one can alter the dihedral angle between the amide group and the pyridine ring on the amino side and thus modulate the interaction between the neighboring pyridines [7].
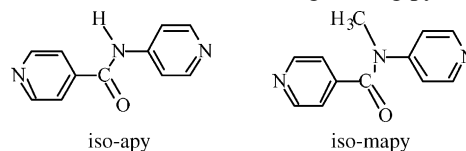
iso-apy   iso-mapy

In this paper, the spectroscopic (MLCT and MMCT) and electrochemical properties of the ruthenium 4-pyridyl isonicotinamide (*iso*-apy) and methyl,4-pyridyl isonicotinamide (*iso*-mapy) were used to calculate electron transfer rate constants. Taking advantage of the difference in electronic structures between the two ruthenium centers, direct kinetic experiments using electron pulse radiolysis were used to determine the rate constants for the thermal intramolecular ET reactions (Eq. (4), below). Comparisons of these results show a reasonable convergence between the kinetic and spectroscopic methods for calculating the thermal rates of intramolecular electron transfer. Finally, the bridging amides will be compared to an extensive list of related complexes with dipyridyl-terminated saturated and unsaturated hydrocarbon bridges as well as with heteroatom bridges separating pyridine rings.

2. Experimental

2.1. Materials

HPLC grade reagents (Fisher Scientific) were used for all reactions unless otherwise noted. The solvents, DMF (spectrophotometric grade), *N*-methyl morpholine, diisopropyl ethylamine (DIEA), triethylamine (TEA) (redistilled) and deuterated solvents, 99.9% D (all from Aldrich), were used without purification. The argon used was from JWS Technologies Inc. All other inorganic and organic chemicals were reagent grade and were used as supplied. The CH$_2$Cl$_2$ (HPLC grade) used in coupling reactions was distilled from calcium hydride. Column chromatography was carried out using silica gel (Acros Organics 0.035–0.07 mm),

Sephadex SP C-25 (Pharmacia Biotech) and CM-32 (Whatman Biosystems Ltd.). The [Ru(NH$_3$)$_5$Cl]Cl$_2$ was prepared from the [Ru(NH$_3$)$_6$]Cl$_3$ (Strem Chemicals), and [Ru(NH$_3$)$_4$SO$_2$Cl]Cl was prepared according to literature procedures [21,22]. Europium oxide, 99.99% (Ventron Alfa), was used to prepare Eu^{3+} solutions in dilute trifluoroacetic (TFA) acid which was reduced with zinc amalgam to generate solutions of Eu^{2+}.

2.2. Instrumentation

Ultraviolet–visible (UV–vis) spectra of the complexes were recorded on a Hewlett-Packard (Model 8452A) diode array spectrophotometer. Visible/near-infrared (visible/NIR) spectra were recorded on a computer-interfaced AVIV spectrophotometer constructed around Cary Model 14 optics. Proton NMR spectra in CDCl$_3$ were recorded on a Varian 200 or 400 MHz spectrometer. All chemical shifts are reported in ppm downfield from tetramethylsilane. Electrospray mass spectrometry (ESMS) analysis was carried out on a Finnigan LCQ-Duo MS using an ion spray source operating in positive ion mode at a voltage of 75 eV. Samples were dissolved in methanol or 5% aqueous acetic acid and introduced via flow injection. Analyte concentrations ranged from 20 to 40 μM.

2.3. Electrochemical measurements

Cyclic voltammetry (CV) and Osteryoung square wave voltammetry (OSWV) were recorded using a BAS 100A electrochemical analyzer (Bioanalytical Systems, West Lafayette, IN). The measurements were carried out in argon-purged solutions using a conventional three-electrode glass cell consisting of a glassy carbon working electrode, a platinum wire auxiliary electrode and a saturated sodium chloride calomel reference electrode (SSCE). The cyclic voltammogram scan rates were 50–100 mV s^{-1}. Before each measurement, the working electrode was freshly polished with a 0.03 mm alumina slurry (Union Carbide) and washed with the appropriate solvent. Redox potentials were determined in water with sodium chloride as the electrolyte.

2.4. Spectral analysis and band fitting

Absorption spectra were resolved into multiple bands using the standard peak measurement and fitting macros provided in Igor Pro software (Wavemetrics, Lake Oswego, OR). All absorption bands were assumed to have a Gaussian shape as a function of energy and their peak positions, widths and amplitudes were allowed to float. OSWV scans for binuclear complexes were resolved into two peaks using customized Igor Pro fitting macros as previously described [23] and adapted to fit OSWV peak functions [24]. For the ruthenium pentaammine derivatives, the OSWV peaks were fit as Gaussian shaped bands with fixed width at half height of 90 mV.

2.5. Preparation of 4-pyridyl isonicotinamide (iso-apy)

Isonicotinic acid (2.470 g, 0.0201 mol) was added to fresh thionyl chloride (10 mL) in a 100 mL round bottom flask. To this, four drops of DMF were added and the mixture was allowed to reflux for 1 h under argon. The solution was concentrated to form a dry white solid using a rotary evaporator. Since isonicotinyl chloride is moisture sensitive, special precautions were taken to avoid exposure to the atmosphere, and the intermediate was used directly for the next step. The isonicotinyl chloride was taken up in dry THF (20 mL); then TEA (3 mL) and 4-aminopyridine (apy) (1.795 g, 0.0191 mol) were added to it. The yellow mixture was allowed to stir for 2 h under argon. After that, 10% NaHCO$_3$(aq) was slowly added to the reaction mixture until the pH of the solution was 9. The crude mixture was purified via solvent extraction (CH$_2$Cl$_2$/H$_2$O), followed by column chromatography (silica gel, 5% MeOH/CH$_2$Cl$_2$) to give a white crystalline solid, mp 188–192 °C. Yield 0.973 g (34%). TLC in 5% MeOH/CH$_2$Cl$_2$: R_f for apy = 0.05, R_f for iso-apy = 0.35.

^{1}H NMR (CDCl$_3$): δ 7.615–7.630 ppm (d, 2H of pyridine); δ 7.712–7.725 ppm (d, 2 H of pyridine); δ 8.150 ppm (s, 1 H of amide); δ 8.587–8.602 ppm (d, 2 H of pyridine); δ 8.837–8.851 ppm (d, 2 H of pyridine). ESMS: obs'd 200.3, calc'd 119.2.

2.6. Preparation of methyl,4-pyridyl isonicotinamide (iso-mapy)

Preparation of 4-methylaminopyridine (mapy): A mixture of 4-chloropyridine hydrochloride (5 g, 33.33 mmol), CuSO$_4$ (33.33 mmol) and methylamine (40 wt% aq, 20 mL) was sealed in a glass tube and heated at 155 °C in a sand bath for 20 h. The resulting blue solution was slowly mixed with 1 M NaOH (250 mL) to precipitate Cu(OH)$_2$, which was filtered off and the filtrate extracted with a 1:1 CH$_2$Cl$_2$/H$_2$O mixture (3 × 100 mL). The organic layer was concentrated to dryness on a rotary evaporator and the product was precipitated from ether as a white crystalline solid, mp 119–122 °C. Yield 2.3 g (65%). TLC in 5% MeOH/CH$_2$Cl$_2$: R_f for 4-chloropyridine = 0.56, R_f for mapy = 0.08. ^{1}H NMR (CDCl$_3$): δ 2.786–2.799 ppm (d, 3H of methyl); δ 6.361–6.373 ppm (d, 2 H of pyridine); δ 8.121–8.134 ppm (d, 2 H of pyridine). ESMS: obs'd 109.3, calc'd 108.1.

The mapy prepared above (0.140 g, 1.3 mmol) and isonicotinyl chloride hydrochloride (1.9 mmol) were placed in a round bottom flask. Dry CH$_2$Cl$_2$ (10 mL), then DIEA (0.7 mL) were added and the yellow solution was stirred for 1 h under N$_2$. After that, additional isonicotinyl chloride hydrochloride (1.3 mmol) and DIEA (0.35 mL) were added to the reaction mixture. The solution was allowed to stir for 12 h and was then concentrated to dryness by rotary evaporation. The residue was taken up in 1% NaHCO$_3$ (aq) and extracted with CH$_2$Cl$_2$. The organic layer was purified by column chromatography (silica gel, 5% MeOH/CH$_2$Cl$_2$) to generate a

yellow oil. Yield 0.164 g (59%) TLC in 5% MeOH/CH$_2$Cl$_2$: R_f for mapy = 0.08, R_f for isonicotinyl chloride = 0.04, R_f for *iso*-mapy = 0.38. ^{1}H NMR (CDCl$_3$): δ 3.528 ppm (s, 3 H of methyl); δ 6.971–6.986 ppm (s, 2 H of pyridine); δ 7.188–7.203 ppm (d, 2 H of pyridine); δ 8.490–8.505 ppm (d, 2 H of pyridine); δ 8.558–8.573 ppm (d, 2 H of pyridine). ESMS: obs'd 214.2, calc'd 213.2.

2.7. [((NH$_3$)$_5$Ru)$_2$-iso-apy](PF$_6$)$_4$ and [((NH$_3$)$_5$Ru)$_2$-iso-mapy](PF$_6$)$_4$

To a 0.1 M HTFA solution, [Ru(NH$_3$)$_5$Cl]Cl$_2$ (3 equiv. to desired amount of ligand) was added and degassed in an argon atmosphere. The degassed mixture was reduced for 1.5 h over zinc amalgam. The reduced ruthenium solution was then added to a degassed buffered solution of the ligand (prepared by adding one drop of HTFA to the desired amount of ligand and then adjusting the pH to 8 with 1 M NaHCO$_3$). The mixture was stirred under argon for 1 h, quenched with DMSO, and the resulting red solution was purified using column chromatography (Sephadex SP C-25). These binuclear species were purified by column chromatography immediately after preparation, since the ruthenium apy bond in these compounds aquates over time to form the mononuclear species. Water was used to elute any water soluble organic compounds from the Sephadex column. Unreacted ruthenium compounds were then removed with 0.1–0.4 M NaCl. The mononuclear species, on *iso* end, was removed with 0.4–0.5 M NaCl and the binuclear ruthenium complex was eluted with 1 M NaCl. The product was concentrated to dryness on a rotary evaporator, taken up in a minimum amount of distilled water, re-reduced over zinc amalgam for 30 min and precipitated by the addition of solid NH$_4$PF$_6$ to form a red solid. Yield ~75% for each ligand.

2.8. Preparation of the bis(pentaammineruthenium(III)) derivatives [((NH$_3$)$_5$Ru)$_2$-**L**](BF$_4$)$_6$, where **L** = iso-apy, iso-mapy

The PF$_6$$^-$ salt from above was dissolved in a minimum amount of HBF$_4$ (48% aqueous) and swirled for 1–2 min. H$_2$O$_2$ was added drop wise until the mixture turned yellow and the solution was slowly added to a stirring solution of acetone. A yellow precipitate formed almost immediately. Yield > 95%.

2.9. [(NH$_3$)$_5$Ru-iso-apy-Ru(NH$_3$)$_4$(methyl imidazole)](PF$_6$)$_4$

To an aqueous solution of [(NH$_3$)$_5$Ru-*iso*-apy](PF$_6$)$_2$ (107 mg) and NaHCO$_3$ (23 mg), [(NH$_3$)$_4$Ru(SO$_2$)Cl]Cl (107 mg) was added and the resultant solution was allowed to react for 30 min under argon. After that, concentrated HCl (three drops) and H$_2$O$_2$ were added until the reaction mixture turned yellow. Acetone was added to precipitate a yellow crystalline solid of [(NH$_3$)$_5$Ru-*iso*-apy-

Ru(NH$_3$)$_4$(SO$_4$)]$^{4+}$. Yield 137 mg (76%). To an aqueous solution of [(NH$_3$)$_5$Ru-*iso*-apy-Ru(NH$_3$)$_4$(SO$_4$)]$^{4+}$ (70 mg) and ascorbic acid (1 equiv.), methyl imidazole (imMe) (0.2 mL) was added. The mixture was allowed to stir under argon for 1.5 h and the resulting red solution was purified by column chromatography as stated above (Sephadex SP C-25). The desired product was eluted between 0.7 and 1.0 M NaCl. The product was purified from NaCl by dissolution in methanol. The product was obtained as an impure purple-pink chloride salt. The solid was dissolved in a minimum amount of distilled water, reduced over zinc amalgam for 30 min, and precipitated to form a red solid by addition of solid NH$_4$PF$_6$.

3. Generation of the mixed-valence species

3.1. Ruthenium derivatives

3.1.1. Method 1

Solutions of bis(pentaammineruthenium(II)) ligand complexes (as PF$_6$$^-$ salts) were prepared by dissolving the compounds in a 1:3 mixture of D$_2$O/CH$_3$CN (for *iso*-apy) or D$_2$O/acetone (for *iso*-mapy) and diluting to the desired concentration with the organic solvent (0.4 mL of 2.5 mM and 4.5 mM, respectively). Stoichiometric amounts (0.1 equiv.) of a 0.1 M solution of ammonium hexanitro cerate (IV) in acetone were transferred to the ruthenium solution via a gas tight syringe and the UV–vis/NIR spectra were recorded after each addition using a 0.1 cm quartz cell. The titration was carried out in the 1:3 (v/v) mixtures of D$_2$O/CH$_3$CN or D$_2$O/acetone in order to dissolve the NH$_4$PF$_6$, since a precipitate formed (assumed to be a cerium hexafluorophosphate salt) when the titration was carried out in D$_2$O.

3.1.2. Method 2

In a 0.1 cm quartz cell, aliquots (0.1 equiv.) of 0.01 M degassed ascorbic acid were added to a 1 mM solution of [(NH$_3$)$_5$Ru-*iso*-apy-Ru(NH$_3$)$_4$(imMe)](PF$_6$)$_6$ in CH$_3$CN. The UV–vis/NIR spectrum was recorded after each addition. In all cases, the concentration of binuclear ruthenium species was directly determined and compared to that calculated from the amount of the titrant needed to generate the mixed-valence species (this is a lower limit of the true concentration, especially for the mixed-valence species with small comproportionation constants, and therefore represents a small overestimate [6]).

3.2. Pulse radiolysis experiments

Fast transient absorption pulse radiolysis experiments were carried out at the Brookhaven National Laboratory Laser-Electron Accelerator Facility (LEAF) [25]. The LEAF radio-frequency photocathode electron accelerator was used

to generate 8.7 MeV electron pulses of <120 ps duration. A pulsed xenon arc lamp was used as the detection light source. Bandpass filters (40 nm) were used to select the analyzing light wavelength. Transient absorption signals were collected with a FND-100 silicon photodiode and digitized with a Tektronix TDS-680B oscilloscope using custom software running on a DEC VAXstation 4000 computer. The data were analyzed with Igor Pro software using routines customized at BNL. The ruthenium complexes (4–16 mM) were dissolved in solutions of 0.2 M NaHCO$_2$, 0.1 M CH$_3$CN at pH 3.5 or 0.4 M NaHCO$_2$, 0.1 M CH$_3$CN at pH 6.0, placed in a 0.1 cm Suprasil spectrophotometer cell, and saturated with N$_2$O gas. The measurements were performed at 21 °C. The dose per pulse was determined by thiocyanate dosimetry and ranged from 15 to 25 Gy.

4. Results

4.1. Synthesis and characterization

The ligands were prepared by coupling the acyl chloride of isonicotinic acid to apy or mapy. Yields of 40–60% were obtained when freshly distilled thionyl chloride was used. The bridging ligands were purified via solvent extraction and column chromatography (see experimental) and characterized by ^{1}H NMR and electrospray MS. Both mononuclear and binuclear ruthenium complexes were purified by ion-exchange (Sephadex SP C-25 and/or CM-32 resins). The complexes were characterized by electrochemistry and UV–vis/NIR spectroscopy. The binuclear species were further characterized from the different electrochemical properties of the amino and carbonyl ends, and their behavior on ion-exchange columns where 0.8–1.0 M NaCl (or 0.8 M HCl) was required for their elution. The corresponding mononuclear complexes were eluted from the same columns with 0.2–0.5 M NaCl (or 0.3–0.5 M HCl).

4.2. Electrochemistry

Cyclic and Osteryoung square wave voltammetry were carried out directly on the ion exchange chromatography eluents. This was particularly important for the aminopyridine–ruthenium complexes due to their propensity to dissociate and release aquopentaammineruthenium(II). The mononuclear species show that when the ruthenium ion is bound to the aminopyridine side of the bridge, the redox potential is more negative than when the metal ion is bound to the isonicotinyl end of the ligand. The CV and OSWV scans of the binuclear complexes show the presence of overlapping one-electron waves for the two different metal centers. This is compared with the single bands obtained for the different mononuclear complexes. The electrochemical data are summarized in Table 1 and the OSWV scans for the ruthenium complexes are shown in Fig. 1.

Table 1

Osteryoung square wave peak reduction potentials for mononuclear and binuclear ruthenium(II,III) complexes (0.1 M NaCl, volts vs. SSCE)

$(NH_3)_5M-N$ ... $N-M'(NH_3)_4L$

Complex number	M	E_{peak}, M$^{III/II}$	M'L	E_{peak}, M'$^{III/II}$
	R = H			
1	Ru	0.136	–	–
	–	–	Ru(NH$_3$)	0.008
3, 9, 4	Ru	0.114	Ru(NH$_3$)	−0.007
10	Ru	0.118	Ru(imMe)	0.014
	R = CH$_3$			
5	Ru	0.093	–	–
	–	–	Ru(NH$_3$)	0.014
7, 11, 8	Ru	0.077	Ru(NH$_3$)	0.002

4.3. UV–vis and NIR spectra

UV–vis data for the binuclear species (Table 2) show a low energy band that is characteristic of a metal-to-ligand charge transfer (MLCT) transition. The higher energy bands for the complexes are consistent with ligand-centered $\pi \rightarrow \pi^*$ transitions. The mononuclear pentaammine ruthenium complexes (carbonyl end) undergo a color change upon protonation and their MLCT bands shift to lower energy (20 nm for iso-apy and 40 nm for iso-mapy). Visible/NIR spectra data show charge transfer bands of the mixed valence ruthe-

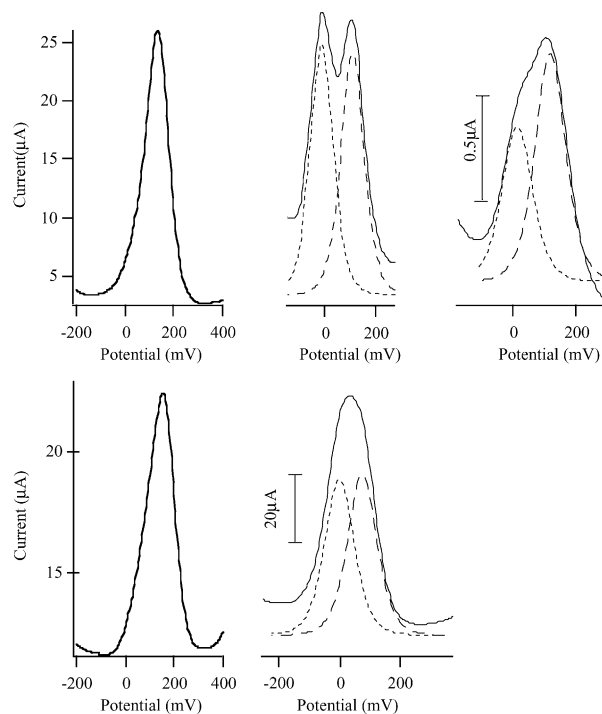Fig. 1. Osteryoung square wave voltammograms of [(NH$_3$)$_5$Ru-iso-apy]$^{n+}$ (carbonyl end), [((NH$_3$)$_5$Ru)$_2$-iso-apy]$^{n+}$, and [(NH$_3$)$_5$Ru-iso-apy-Ru(NH$_3$)$_4$(imMe)]$^{n+}$ (top row), [(NH$_3$)$_5$Ru-iso-mapy]$^{n+}$ (carbonyl end) and [((NH$_3$)$_5$Ru)$_2$-iso-mapy]$^{n+}$ (bottom row). Calculated (- - -) and experimental (—) band shapes (assuming Gaussian waves with half-height widths of 90 mV).

Table 2
UV–vis spectra for mononuclear and binuclear ruthenium complexes (λ_{max}, nm (ε_{max}, M^{-1} cm^{-1}))

$(NH_3)_5M-N$ ... $N-X$ (structure with O, N, R)

M	X	Complex number	R = H	Complex number	R = CH₃
Ru^{II}	–	**1**	202 (32500), 268 (22000), 500 (10500)	**5**	200 (18000), 258 (9500), 466 (5200)
Ru^{II}	H$^+$	**2**	188, 279, 520	**6**	210, 276, 504
Ru^{II}	Ru^{II}(NH$_3$)$_5$	**3**	226 (10250), 256 (8140), 322 (sh), 500 (10130)	**7**	206 (7500), 254 (6500), 464 (7600)
Ru^{III}	Ru^{III}(NH$_3$)$_5$	**4**	236 (12700), 292 (9200), 322 (sh), 422 (1825)	**8**	212 (4250), 322 (7050), 484 (sh)

Table 3
Intervalence spectra for the mixed valence binuclear ruthenium complexes (λ_{max}, nm (ε_{max}, M^{-1} cm^{-1}) (λ_{max}, cm^{-1}))

$(NH_3)_5M-N$ ... $N-X$ (structure with O, N, R)

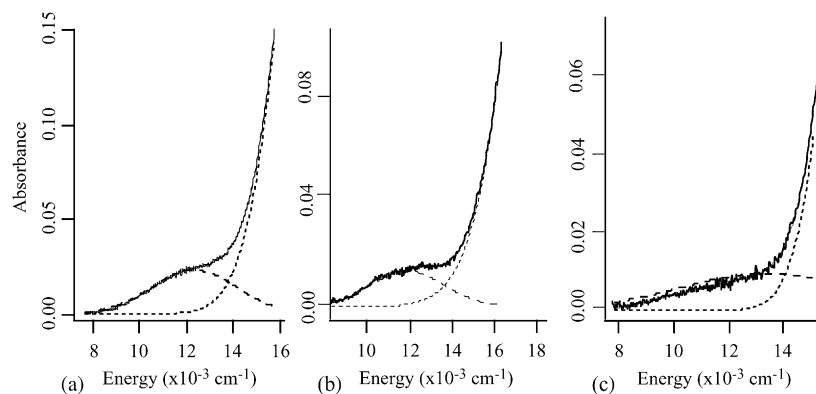| M	X	Complex number	R = H	Complex number	R = CH₃
Ru^{II}	Ru^{III}(NH$_3$)$_5$	**9**	809 (50) (12300)[a]	**11**	743 (20) (13400)[a]
Ru^{II}	Ru^{III}(NH$_3$)$_4$(imMe)	**10**	833 (100) (12000)		

[a] Obtained in D$_2$O/CH$_3$CN for R = H and D$_2$O/acetone for R = CH$_3$ from PF$_6^-$ derivative.

Fig. 2. Calculated (- - -) and experimental (—) band shape for the MMCT bands of the PF$_6^-$ salts of: (a) [((NH$_3$)$_5$Ru)$_2$-*iso*-apy]$^{5+}$, (b) [(NH$_3$)$_5$Ru-*iso*-apy-Ru(NH$_3$)$_4$(imMe)]$^{5+}$ and (c) [((NH$_3$)$_5$Ru)$_2$-*iso*-mapy]$^{5+}$, plotted on an energy scale. Fitted absorption bands were assumed to be Gaussian in shape and width at half height was allowed to float.

nium(II,III) binuclear complexes (Table 3). For the mixed valence ruthenium complexes, **9**–**11**, weak, low energy bands appear at the tail of MLCT bands. Such bands are not present in the spectra of the fully oxidized or reduced complexes (Fig. 2).

5. Kinetic measurements

The kinetics of intramolecular ET in the binuclear [(NH$_3$)$_5$Ru)$_2$-**L**](BF$_4$)$_6$ complexes, where **L** = *iso*-apy and *iso*-mapy were determined using electron pulse radiolysis transient absorption spectroscopy. Electron-irradiated water primarily forms $^\bullet$OH, H$^\bullet$ and e$_{aq}^-$ species; the latter two can be converted to equivalents of $^\bullet$OH through reaction

with aqueous N$_2$O. In 1 M sodium formate saturated with N$_2$O, the predominant $^\bullet$OH species abstracts a hydrogen atom from formate anion to produce the strongly reducing radical, CO$_2^{\bullet-}$. These reactions are shown in Eqs. (1) and (2):

$$H_2O \rightarrow e_{aq}^- + {}^\bullet OH + H^\bullet \tag{1}$$

$$^\bullet OH + HCO_2^- \rightarrow H_2O + CO_2^{\bullet-} \tag{2}$$
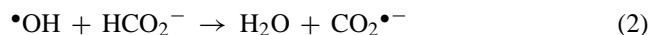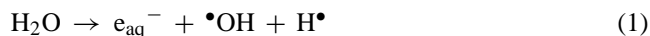
The CO$_2^{\bullet-}$ radical can reduce either metal center in the binuclear [(NH$_3$)$_5$Ru^{III}-**L**-Ru^{III}(NH$_3$)$_5$]$^{6+}$ complex (Eq. (3)), resulting in a population of the kinetic intervalence intermediate reduced at the apy end. Rate constants for intramolecular electron transfer (Eq. (4)) are obtained by monitoring the growth of the absorbance at λ = 500–600 nm from the ruthenium(II) complex at the *iso* end of the bridge. The [(NH$_3$)$_5$Ru^{III}-**L**-
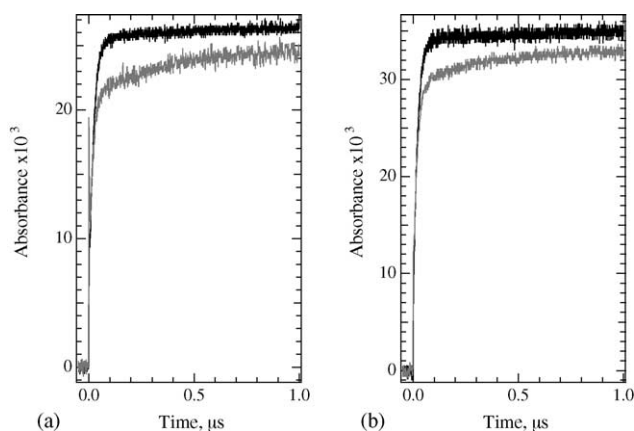
Fig. 3. (a) Absorbance vs. time data for the reduction of $[(NH_3)_5Ru^{III}\text{-}L\text{-}Ru^{III}(NH_3)_5]$ with $CO_2^{\bullet-}$ monitored at: (a) 550 nm and (b) 500 nm. In each graph, the upper, black trace corresponds to $\mathbf{L} = iso$-apy (7.8 mM) and the lower, gray trace corresponds to $\mathbf{L} = iso$-mapy (7.9 mM). The traces for the iso-mapy complex were scaled by factors of 2.4 and 1.5, respectively, in (a) and (b) to better compare the kinetic behavior of both complexes. Conditions: 0.4 M sodium formate, 0.1 M acetonitrile, pH 6.0, N_2O-saturated aqueous solution, 21 °C, pathlength 0.1 cm, radiolytic dose 25 Gy.

$Ru^{III}(NH_3)_5]^{6+}$ concentrations were varied from 4 to 16 mM to probe for a bimolecular contribution to the observed rate constant. The dependence of the reaction on the concentration of the binuclear ruthenium species is then used to determine the intramolecular ET rate constant corresponding to Eq. (4).
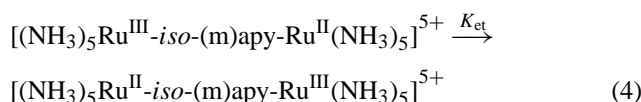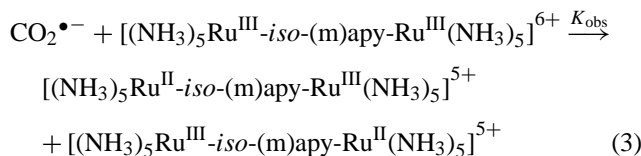
$$CO_2^{\bullet-} + [(NH_3)_5Ru^{III}\text{-}iso\text{-}(m)apy\text{-}Ru^{III}(NH_3)_5]^{6+} \xrightarrow{K_{obs}}$$

$$[(NH_3)_5Ru^{II}\text{-}iso\text{-}(m)apy\text{-}Ru^{III}(NH_3)_5]^{5+}$$

$$+ [(NH_3)_5Ru^{III}\text{-}iso\text{-}(m)apy\text{-}Ru^{II}(NH_3)_5]^{5+} \qquad (3)$$

$$[(NH_3)_5Ru^{III}\text{-}iso\text{-}(m)apy\text{-}Ru^{II}(NH_3)_5]^{5+} \xrightarrow{K_{et}}$$

$$[(NH_3)_5Ru^{II}\text{-}iso\text{-}(m)apy\text{-}Ru^{III}(NH_3)_5]^{5+} \qquad (4)$$

Fig. 3a and b show the pulse radiolysis transient absorption traces for the reduction of $[(NH_3)_5Ru^{III}\text{-}iso\text{-}(m)apy\text{-}Ru^{II}(NH_3)_5]^{6+}$. The kinetic behavior of the two complexes is compared at 550 and 500 nm. The $(NH_3)_5Ru^{II}\text{-}iso$ fragment absorbs more strongly at both wavelengths than the $(m)apy\text{-}Ru^{II}(NH_3)_5$ fragment. In the case of the iso-mapy-bridged complex (gray traces) the initial absorbance increase due to reaction (3) is followed by a further increase due to intramolecular ET (reaction (4)) with a rate constant of $2.7 \pm 0.4 \times 10^6\,s^{-1}$. For the iso-apy-bridged species (black traces), only a single pseudo-first-order process correspond-

ing to reaction (3) is observed over a concentration range of 4.1–32 mM. Therefore, only a lower limit of $\geq 7 \times 10^7\,s^{-1}$ can be estimated for the intramolecular ET rate constant.

6. Discussion

In the ruthenium complexes reported here, both the mixed-valence spectroscopic properties and the kinetics of thermal intramolecular electron transfer of the binuclear complexes can be studied. By making the amide group part of the bridging ligand, the effect of the dihedral angle between the amide group and the pyridine rings on ET rates can be examined.

The differences in chromatographic and electrochemical properties between the mononuclear and binuclear derivatives formed the basis of their characterization (Table 1 and Fig. 1). Dissimilarity of the ligated pyridine rings causes a small difference in the spectroscopic and electrochemical properties of the mononuclear and binuclear complexes. When the metal is attached to the more electron-withdrawing, carbonyl bearing pyridine, a more positive redox potential is observed relative to that of the metal coordinated to the more electron rich aminopyridine ($\sim$100 mV greater). Protonation of the ruthenium(II) mononuclear species **2** and **6** resulted in spectral shifts consistent with charge redistribution of the protonated species (Table 2). Upon protonation at the apy end, a reversible red shift in the MLCT band is observed. The ruthenium pentaammine species undergo a color change upon protonation and their MLCT bands shift to lower energy (770 and 1620 cm^{-1} for iso-apy and iso-mapy, respectively) The difference in charge redistribution can be accounted for using the intermediate structure in Scheme 1. When R $=$ CH$_3$, the positive charge that develops is expected to be more stabilized than for R $=$ H.

The binuclear mixed-valence ruthenium pentaammine derivatives show broad bands assigned to intervalence charge transfer (MMCT) at the lower energy tail of the MLCT bands (iso-apy at 12,300 cm^{-1} and iso-mapy at 13,400 cm^{-1}). These bands are absent from the spectra of the fully oxidized and fully reduced binuclear species. To ascertain the nature of the mixed-valence band, the fully reduced complex $[(NH_3)_5Ru\text{-}iso\text{-}apy\text{-}Ru(NH_3)_4(N\text{-methyl imidazole})](PF_6)_5$ was synthesized and studied. The presence of N-methyl imidazole in place of the trans ammonia at the apy side is expected to increase the potential of this site compared to that of the carbonyl site (Table 1), thus decreasing the energy gap of the intervalence transfer absorption band. As expected, a red shift in the MMCT band for this complex was observed
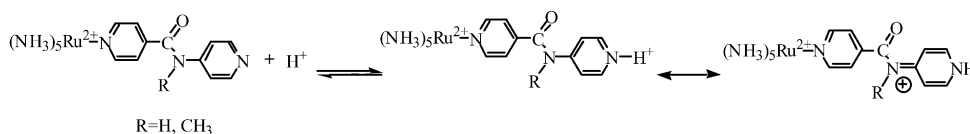
Scheme 1.

Table 4
Spectroscopic parameters and metal–ligand coupling in mononuclear ruthenium complexes

Complex number	λ_{max} (nm)	ν_{max} MLCT (cm^{-1})	ε_{max} (M^{-1} cm^{-1})	$\Delta\nu_{1/2}$ (cm^{-1})	H_{ML} Hush (cm^{-1})
1	500	20000	10000	4300	2800
a	418	23900	7000	4200	2500
5	466	21400	7600	5100	2700

(**a**) The M′L values for all mononuclear ruthenium(II) species (either (NH$_3$)$_5$ or (NH$_3$)$_4$ on apy end) are identical and were obtained from the spectroscopic parameters of (NH$_3$)$_5$Ru^{II}-aminopyridine-amide [37]. $r_{ML} = 6.85$ Å for all mononuclear species.

relative to the corresponding Ru(NH$_3$)$_5$ (11,900 cm^{-1} versus 12,300 cm^{-1}, respectively, Fig. 2).

The electronic coupling element, $H_{MM'}$, is important for understanding how efficiently the bridging ligand mediates MMCT. It is also related to the thermal rate of ET. The variation in electronic coupling with angular dependence for the ruthenium complexes **9** and **11** was studied by comparing the energy and absorptivity of the two MMCT bands (Fig. 2). By replacing the H of the amide with a methyl group, the dihedral angle between the apy ring and the amide bond changes by ~40° [26], thereby changing the MLCT and MMCT band energies (Table 4). A significant decrease in $H_{MM'}$ accompanies this change (Table 5). The MLCT and MMCT bands (assigned from the spectra) were used to calculate the electronic coupling elements H_{ML} and $H_{MM'}$ (for metal-to-ligand and metal-to-metal, respectively) using Hush [27,28] and CNS methods [29]. The results in Tables 4 and 5 indicate that the *iso*-apy bridge shows more effective coupling than *iso*-mapy for all of the complexes studied. However, some discrepancy still exists between the electronic coupling values obtained from the two methods. The CNS calculation results in effectively no difference in coupling between the R = H and CH$_3$ cases, however there is at least a factor of 10 difference in the kinetically-determined intramolecular electron transfer rate constants. In the CNS formalism, direct metal-to-metal coupling is neglected, and mixing with only one MLCT state is considered. However, in the case of the complexes reported here, the character of the MLCT and M'LCT states is mostly localized to the respective pyridine rings bound to each metal center. This distinction may be responsible for the larger divergence between the couplings $H_{MM'}$ calculated by the Hush and CNS methods compared to the examples given in [29], where agreements were within a factor of two. In addition, refinement of these calculations using results from electroabsorption spectroscopy may further resolve some of the differences [30].

The *iso*-mapy derivative showed an intramolecular ET rate of $2.7 \pm 0.4 \times 10^6$ s^{-1}. This rate was slower than the initial reduction of Ru(III) by the reducing radical ($\sim 3 \times 10^7$ s^{-1}). (Fig. 3a). To confirm the intramolecular nature of the slower rate constant, the concentration of the binuclear complex was changed from 4 to 8 mM. The kinetics showed that the faster, bimolecular rate constant increased by a factor of 1.8 (to $\sim 5.5 \times 10^7$ s^{-1}), while no change was observed for the slower intramolecular ET rate constant. The concentration independence of the second rate constant supports its assignment to the intramolecular ET reaction from the Ru^{II} on the amino end to the Ru^{III} on the carbonyl end.

Experiments on the *iso*-apy-bridged complex did not show two distinguishable rate constants (Fig. 3b). As the concentration was increased from 4.1 to 32 mM, the bimolecular rate increased but was not separated from the intramolecular ET rate constant. Therefore, the data provides only a lower limit for k_{et} of $\geq 7 \times 10^7$ s^{-1}. To achieve a clearer separation between kinetic steps, the reaction would have to be carried out at a higher concentration of the binuclear species. However since the solubility limits have been reached, changing the anion to form a more soluble compound may be required.

The novelty of these mixed-valence systems lies in the fact that electron transfer rate constants can be calculated from spectroscopic MMCT bands [10] and directly measured by fast kinetic methods. Therefore a direct comparison between the two methods is possible using Eqs. (5) and (6) [10,28], assuming 5×10^{12} to be an average frequency that

$$k_{et} = 5 \times 10^{12} \, e^{-(\Delta G^*/RT)} \tag{5}$$

$$\Delta G^* = \frac{E_{op}}{4} - H_{MM} - \Delta G^0 \tag{6}$$

accounts for metal-to-ligand and solvent frequencies (non-adiabatic reactions), E_{op} is the optical energy for MMCT, $H_{MM'}$ is the electronic coupling element for MMCT, and ΔG^0 is the driving force of the reaction. Using $H_{MM'}$ values

Table 5
Comparison of observed and calculated metal–metal coupling parameters in [((NH$_3$)$_5$M)$_2$-L]$^{5+}$ and [((imMe)(NH$_3$)$_4$Ru-*iso*-apy-Ru(NH$_3$)$_5$)]$^{5+}$ mixed-valence complexes

Complex number	λ_{max}[a] (nm)	ν_{max} MM′CT (cm^{-1})	ε_{max} (M^{-1} cm^{-1})	$\Delta\nu_{1/2}$[b] (cm^{-1})	ΔE_{ML} (cm^{-1})	$H_{M'M'}$ Hush (cm^{-1})	$H_{MM'}$ CNS (cm^{-1})
9	809	12400	50	5100	11000	90	320
11	743	13500	20	5500	11500	60	290
10	833	12000	100	5000	11400	100	300

$r_{MM'} = 13.7$ Å for all binuclear species.

[a] The IT band was obtained from the Gaussian fits.

[b] The values reported were corrected for symmetry using the equation [38] $\Delta\nu_{1/2} = (2310 \, (\nu_{max} - \Delta G^0 \, (cm^{-1})))^{1/2}$.

obtained [40] by Hush's method, the calculated values for k_{et} are $3 \times 10^8 \, s^{-1}$ (for *iso*-apy) and $1 \times 10^7 \, s^{-1}$ (for *iso*-mapy). The pulse radiolysis experiments obtained a lower limit for the intramolecular electron transfer rate constant k_{et} of $7 \times 10^7 \, s^{-1}$ in the case of *iso*-apy and $k_{et} = 2.7 \pm 0.4 \times 10^6 \, s^{-1}$ for *iso*-mapy. The experimentally determined rate constant and lower limit are more than three times slower than the estimated ones, but trends are consistent between the two approaches. The mixed-valence complex $[(NH_3)_5Ru^{II}\text{-pyrazine-}Ru^{III}(edta)]^+$ has been used previously for comparing intervalence spectroscopy and thermal electron transfer, [31] although in that case the calculated ET rate constant was over 50 times faster than the observed value.
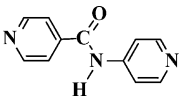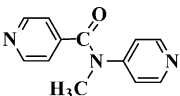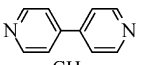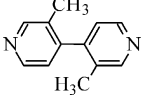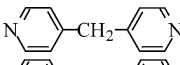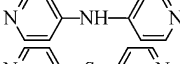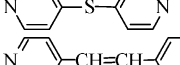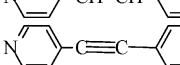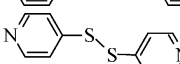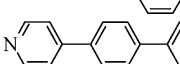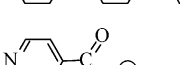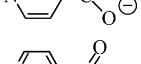
6.1. Comparison to bridging saturated and unsaturated hydrocarbon bridges and with similar bridging ligands
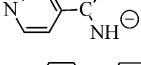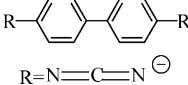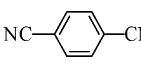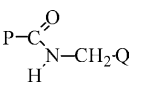
The ruthenium complexes reported here possess similar electron mediating properties to that of many dipyridyl-terminated bridging ligands. Furthermore, the dihedral angle between the amino pyridine ring and the amide group also influences MMCT coupling. A comparison of the mediating properties of the amide group (with different dihedral angles) can be made to a number of similar functional groups already studied. To examine the dependence of the electronic coupling on the orientation of the pyridine rings, Taube and coworkers [7,32] compared mixed-valence binuclear pentaammineruthenium complexes bridged by 4,4′-bipyridine and 3,3′-dimethyl-4,4′-bipyridine. In the latter compound, the methyl groups cause the pyridine rings to form a larger dihedral angle in comparison to 4,4′-bipyridine. The MMCT band energy increased with dihedral angle (1050 nm versus 860 nm) which resulted in a decrease in $H_{MM'}$ by a factor of 2 (Table 6). In the amide systems reported here, $H_{MM'}$ values decreased by a factor of 1.5 as the result of one methyl group placed at the amide nitrogen.

Earlier studies have explored the properties of deprotonated carboxylic acids and amides in isonicotinato and isonicotinamido ligands and their binuclear ruthenium complexes [33] (Table 6). The isonicotinamido ligand has a deprotonated amide group directly bound to the Ru(III) center. Both isonicotinamido and isonicotinato ligands showed similar spectral properties, but the electronic coupling in the isonicotinamido ligand was found to be 1.7 times larger than that of the isonicotinato ligand ($520 \, cm^{-1}$ versus $300 \, cm^{-1}$). Early work by Liu and Bolton [34] also addressed the mediation properties of amide bonds connected to a methylene group (an amino acid bridging group). The electronic coupling between the donor porphyrin and an acceptor benzoquinone is significantly decreased in the presence of the additional methylene group (Table 6).

When compared to other dipyridyl-terminated systems coupled through two-atom linkages, the amide-coupled metal complexes show less efficient coupling than olefinic, acetylenic and disulfide groups. The amide systems can also be compared to complexes with single-atom bridges (S, NH

Table 6
Comparison of $H_{MM'}$ values to related literature values

Ligand	r_{MM} (Å)	$H_{MM'}$ ($10^3 \, cm^{-1}$) (solvent)	Reference
(N-pyridyl–C(=O)–N(H)–pyridyl-N)	13.7	0.09 (D_2O/CH_3CN)[a] 0.32 (D_2O/CH_3CN)[b]	This work
(N-pyridyl–C(=O)–N(CH₃)–pyridyl-N)	13.7	0.06 (D_2O/acetone)[a] 0.29 (D_2O/acetone)[b]	This work
(N-pyridyl–pyridyl-N, CH₃)	11.3	0.39 (0.1 M DCl/D_2O)[a] 0.60 (0.1 M DCl/D_2O)[b]	[32]
(N-pyridyl–pyridyl-N, H₃C)	11.3	0.19 (0.1 M DCl/D_2O)[a]	[32]
(N-pyridyl–CH_2–pyridyl-N)	10.5	0.10 (0.1 M DCl/D_2O)[a]	[32]
(N-pyridyl–NH–pyridyl-N)	10.9	0.50 (0.1 M DCl/D_2O)[a]	[32]
(N-pyridyl–S–pyridyl-N)	~11	~0.15 (D_2O)[a]	[7,10]
(N-pyridyl–CH=CH–pyridyl-N)	13.8	0.30 (0.1 M DCl/D_2O)[a]	[32]
(N-pyridyl–C≡C–pyridyl-N)	14.0	0.29 (0.1 M DCl/D_2O)[a]	[32]
(N-pyridyl–S–S–pyridyl-N)		0.855 (D_2O)[a]	[13,39]
(N-pyridyl–phenyl–pyridyl-N)	15.6	~0.20 (DMSO(d_6))[a,e] ~0.50 (DMSO$-d_6$)[b,e]	[15]
(N-pyridyl–C(=O)–O⁻)	9.0	0.30 (0.1 M KCF_3SO_3)[a]	[33]
(N-pyridyl–C(=O)–NH⁻)	9.2	0.52 (0.1 M KCF_3SO_3)[a] 0.80 (0.1 M KCF_3SO_3)[b]	[29]
(R–phenyl–phenyl–R, R = N=C=N⁻)	17.2[c]	0.36 (CH_3CN)[a]	[35]
(NC–phenyl–CN)	11.8	0.32 (1 M D_2SO_4)	[9]
(P–C(=O)–N(H)–CH_2–Q)	14.0	0.003 (CH_3CN)	[34][f]

All these species are $[((NH_3)_5Ru)_2\text{-}L]^{5+}$ (except that for [34]). (d) From $H = (\nu_{max} \, \Delta G_r)^{1/2}$, no corrections for ΔG_r were made as K_c is large.
[a] From Hush equation.
[b] From CNS theory.
[c] Distance was calculated by adding 4.2 Å (for phenyl group) to 13.0 Å (for 1,4-dicyanamidobenzene dianion).
[e] Estimated from figures in [15].
[f] P and Q are porphyrin and benzoquinone.

and CH_2) separating the pyridine rings [7,32]. The amine spacer, NH, shows the strongest coupling, followed by the S-atom bridge, while the amide and single CH_2 groups are significantly weaker (Table 6). The electron donation of the NH group is reduced upon interaction with the electron withdraw-

ing carbonyl group resulting in the weaker coupling observed in the amide bridge. The amide system can also be compared to similar dipyridyl complexes with phenyl spacers [15]. The phenyl group-coupled complex showed an MMCT band with slightly lower energy and larger electronic coupling than the amide link, even though the separation distance in the phenyl linker is longer (Table 6). The extended conjugation of the π system of the phenyl group explains this more favorable interaction.

A series of negatively charged ligands (not directly related to amino acids or peptides) designed to enhance electron transfer over longer distances have been reported [35]. In these systems, ligand-to-metal and metal-to-ligand interactions are both important factors in determining the metal-to-metal coupling. These ligands show stronger coupling than either of the amide complexes studied here or the conjugated neutral bridges shown in Table 6. Introducing such negatively charged ligands into amide bonds could enhance extended electronic mediations.

In conclusion, $H_{MM'}$ values for amide complexes with ruthenium donors and acceptors have been successfully determined from spectroscopic and kinetic measurements. The rather weak observed intervalence charge transfer bands indicate that in more extended peptide-bridged complexes (where lower electronic coupling is expected), $H_{MM'}$ values are more likely to be determined from direct kinetic measurements of ET rate rather than from spectroscopic MMCT bands [36].

Acknowledgements

References

[1] P. Ford, R.G. Gaunder, E.P. De Rudd, H. Taube, J. Am. Chem. Soc. 90 (1968) 1187.
[2] C. Creutz, H. Taube, J. Am. Chem. Soc. 91 (1969) 3988.
[3] H. Taube, Pure and Appl. Chem. 51 (1979) 901.
[4] P.A. Lay, R.H. Magnuson, J.P. Sen, H. Taube, J. Am. Chem. Soc. 104 (1982) 7658.
[5] P.A. Lay, R.H. Magnuson, H. Taube, Inorg. Chem. 27 (1988) 2364.
[6] J.E. Sutton, P.M. Sutton, H. Taube, Inorg. Chem. 18 (1979) 1017.
[7] H. Fischer, G.M. Tom, H. Taube, J. Am. Chem. Soc. 98 (1976) 5512.
[8] D. Richardson, H. Taube, Coord. Chem. Rev. 60 (1984) 107.
[9] D.E. Richardson, H. Taube, J. Am. Chem. Soc. 105 (1983) 40.
[10] C. Creutz, Prog. Inorg. Chem. 30 (1983) 1.
[11] W. Kaim, A. Klein, M. Glockle, Acc. Chem. Res. 33 (2000) 755.
[12] S.S. Isied, in: H. Sigel, A. Sigel (Eds.), Metals in Biological Systems, vol. 27, Marcel Dekker Inc., New York, 1991, p. 1.
[13] R.J. Crutchley, Adv. Inorg. Chem. 41 (1994) 273.
[14] I.D.S. Moreira, D.W. Franco, J. Chem. Soc., Chem. Comm. (1992) 450.
[15] Y. Kim, C.M. Lieber, Inorg. Chem. 28 (1989) 3990.
[16] S. Woitellier, J.P. Launay, C.W. Spangler, Inorg. Chem. 28 (1989) 758.
[17] R.W. Callahan, G.M. Brown, T.J. Meyer, Inorg. Chem. 14 (1975) 1443.
[18] G.A. Neyhart, J.T. Hupp, J.C. Curtis, C.J. Timpson, T.J. Meyer, J. Am. Chem. Soc. 118 (1996) 3724.
[19] G.A. Neyhart, C.J. Timpson, D. Bates, T.J. Meyer, J. Am. Chem. Soc. 118 (1996) 3730.
[20] G. Giuffrida, S. Campagna, Coord. Chem. Rev. 135/136 (1994) 517.
[21] L. Vogt, J. Katz, S. Wiberly, Inorg. Chem. 4 (1965) 1157.
[22] P.A. Lay, R.H. Magnuson, H. Taube, Inorg. Synth. 24 (1986) 269.
[23] J. Sun, J.F. Wishart, R. van Eldik, R.D. Shalders, T.W. Swaddle, J. Am. Chem. Soc. 117 (1995) 2600.
[24] J. Luo, PhD Dissertation, Rutgers University, 1998, p. 35.
[25] (a) J.F. Wishart, in: C.D. Jonah, B.S.M. Rao (Eds.), Studies in Physical and Theoretical Chemistry, vol. 87, Elsevier Science, New York, 2001, Chapter 2, pp. 21–35 ;
(b) J.F. Wishart, A.R. Cook, J.R. Miller, Rev. Sci. Instrum., in press (doi:10.1063/1.1807004).
[26] K. Krogh-Jespersen, personal communication.
[27] R.S. Mulliken, J. Am. Chem. Soc. 64 (1952) 811.
[28] N.S. Hush, Prog. Inorg. Chem. 8 (1967) 391.
[29] C. Creutz, M.D. Newton, N.J. Sutin, Photochem. Photobiol. A: Chem. 82 (1994) 47.
[30] (a) B.S. Brunschwig, C. Creutz, N. Sutin, Coord. Chem. Rev. 177 (1998) 61;
(b) Y.-G.K. Shin, B.S. Brunschwig, C. Creutz, N. Sutin, J. Phys. Chem. 100 (1996) 8157.
[31] C. Creutz, P. Kroger, T. Matsubara, T.L. Netzel, N. Sutin, J. Am. Chem. Soc. 101 (1979) 5442.
[32] J. Sutton, H. Taube, Inorg. Chem. 20 (1981) 3125.
[33] M.H. Chou, C. Creutz, N. Sutin, Inorg. Chem. 31 (1992) 2318.
[34] J. Liu, J.R. Bolton, J. Phys. Chem. 96 (1992) 1718.
[35] M.S. Aquino, C.A. White, C. Bensimon, J.E. Greedan, R.J. Crutchley, Can. J. Chem. 74 (1996) 2201.
[36] S.S. Isied, A. Vassilian, J.F. Wishart, C. Creutz, H.A. Schwarz, N. Sutin, J. Am. Chem. Soc. 110 (1988) 635.
[37] R. Abdel-Malak, PhD Dissertation, Rutgers University, 2003, p. 78.
[38] R.A. Marcus, N. Sutin, Biochim. Biophys. Acta 811 (1985) 265.
[39] I.D.S. Moreira, D.W. Franco, Inorg. Chem. 33 (1994) 1607.
[40] $RT = 596$ cal at 300 K. For iso-apy; $\Delta G0 = 0.121$ V (976 cm−1), $HMM' = 90$ cm−1, $Eop = 806$ nm (12400 cm−1). For iso-mapy; $\Delta G0 = 0.075$ V (605 cm−1), $HMM' = 60$ cm−1, $Eop = 743$ nm (13459 cm−1).